JACS
JOURNAL OF THE AMERICAN CHEMICAL SOCIETY
Communication
pubs.acs.org/JACS

Homogeneous Nucleation of Methane Hydrates: Unrealistic under Realistic Conditions

Brandon C. Knott,[†] Valeria Molinero,[‡] Michael F. Doherty,[†] and Baron Peters*[,†,§]

[†]Department of Chemical Engineering, University of California, Santa Barbara, California 93106, United States
[‡]Department of Chemistry, University of Utah, Salt Lake City, Utah 84112, United States
[§]Department of Chemistry and Biochemistry, University of California, Santa Barbara, California 93106, United States

Supporting Information

ABSTRACT: Methane hydrates are ice-like inclusion compounds with importance to the oil and natural gas industry, global climate change, and gas transportation and storage. The molecular mechanism by which these compounds form under conditions relevant to industry and nature remains mysterious. To understand the mechanism of methane hydrate nucleation from supersaturated aqueous solutions, we performed simulations at controlled and realistic supersaturation. We found that critical nuclei are extremely large and that homogeneous nucleation rates are extremely low. Our findings suggest that nucleation of methane hydrates under these realistic conditions cannot occur by a homogeneous mechanism.

Clathrate hydrates of natural gases ("gas hydrates") are crystalline inclusion compounds in which methane or other gases are held within a structure of polyhedral cages of water.[1] Gas hydrates are an enormous potential resource of fossil-fuel energy[1] but can also threaten energy supplies by blocking pipelines and exacerbating oil-well blowouts.[2] Additionally, gas hydrates impact global climate trends,[1] carbon dioxide sequestration,[3] and gas storage[4] and transportation.[5,6] Molecular simulations have contributed much to our understanding of gas hydrates, including their phase behavior,[7−10] nucleation,[11−20] growth,[21,22] dissolution,[23−25] and transport properties.[26−28]

Mechanistic hypotheses for the homogeneous nucleation of gas hydrates include assembly of preformed water cages;[20] local ordering of gas molecules followed by cage formation;[17] stabilization of water cages by guest adsorption;[19] and two-step nucleation, which requires initial formation of a concentrated zone of disordered methane.[12,14,15] The evidence for these hypotheses is largely from simulations with extremely high driving forces toward crystallization.

The driving force for gas hydrate nucleation from aqueous solution is supersaturation, that is, an excess concentration of methane in aqueous solution beyond its solubility at the same temperature and pressure. Previous simulations revealed important mechanistic insights, but these were performed at highly elevated supersaturations that might artificially accelerate nucleation and alter the mechanism from that which occurs under natural conditions.[11,12,14,15,17,29] However, simulations at lower, realistic supersaturations are challenging because (1) controlling supersaturation in the condensed phase is difficult and (2) nucleation is a rare event requiring specialized simulation methods. The first challenge can be overcome by including a methane gas reservoir within the simulation cell at constant temperature and pressure, as first demonstrated by Walsh and co-workers.[13,29] The second challenge is exemplified by comparing simulated and experimental nucleation rates. In microsecond simulations, Walsh and co-workers[13,29] computed nucleation rates of $\sim 10^{25}$ nuclei cm^{-3} s^{-1}, the lowest to date of any simulation study of spontaneous hydrate nucleation.[29] However, rate estimates based on experimental induction times (10^{-3}–10^{-7} nuclei cm^{-3} s^{-1}) are almost 30 orders of magnitude lower,[30−35] indicating a continuing need for analysis with rare-events methods at lower supersaturations.

This work used molecular dynamics (MD) simulations for direct computation of the supersaturation as well as the thermodynamic and dynamic properties of hydrate nuclei. The surface energy of critical nuclei was then estimated as a fitting parameter in a least-squares minimization. With these calculated quantities, classical nucleation theory relationships were then utilized to estimate the nucleation barrier, critical nucleus size, and homogeneous nucleation rate. Our results indicate that homogeneous nucleation of clathrate hydrates does not contribute to their crystallization under realistic conditions of formation in industry and nature.

Simulations were performed with the coarse-grained mW water model[36] and united-atom methane,[37] which reproduce the experimental hydration number of methane in water and the melting temperatures of structure I (sI) and structure II (sII) methane hydrates.[37] To describe the high-pressure solubility of methane in aqueous solution accurately, the model's CH_4−CH_4 interactions were modified from their original values [see the Supporting Information (SI)]. Also, the mW model overestimates the diffusivity of water by a factor of ∼4 at 273 K[36] (see the SI for further discussion). We expect that mW in this application similarly enhanced the diffusivity of water and methane, thereby increasing the nucleation prefactor relative to that for fully atomistic water models. Our calculated nucleation rate should therefore be viewed as an upper bound on the actual rate.

All of the simulations were performed in elongated cells containing a methane gas layer with flat interfaces to control supersaturation without Laplace pressure contributions (except for solution/hydrate coexistence simulations, which had no

Received: September 13, 2012
Published: November 13, 2012

dx.doi.org/10.1021/ja309117d | J. Am. Chem. Soc. 2012, 134, 19544−19547

methane gas layer). Simulations of nucleation were performed at T = 273 K and P = 900 atm, where liquid water, not ice, is the metastable parent phase.[38] Below this temperature, there would be a kinetic competition between nucleation of ice and gas hydrate. This model's melting temperature of methane hydrate at 900 atm is 298 ± 2 K, in good agreement with the experimental value (303 ± 1 K).[39] The chosen state point represents a typical temperature and an upper bound on the pressure at locations where gas hydrates are found (e.g., deep sea floor, permafrost, and gas pipelines).

Isothermal−isobaric MD simulations were used to determine the relationship between pressure and supersaturation at 273 K (Figure 1). The supersaturation is defined as $S = c/c_{sat}$, where c is

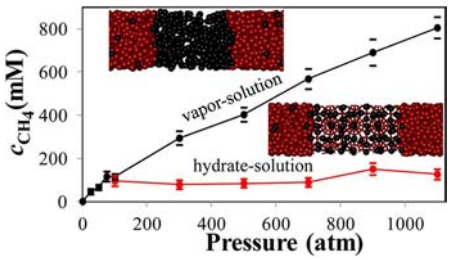

Figure 1. Concentration (mol/m^3) of methane in aqueous solution at 273 K in coexistence with methane gas (top snapshot and black curve) and with hydrate (bottom snapshot and red curve). In the snapshots, red spheres represent water molecules and black spheres represent methane molecules (for clarity, only ∼15% of the solution phase is shown).

the methane concentration in aqueous solution and c_{sat} is the aqueous methane concentration that would be in equilibrium with a gas hydrate. Calculation of the supersaturation therefore requires two simulations at each pressure: (1) aqueous solution in contact with methane gas and (2) aqueous solution in contact with gas hydrate.

Clathrates tile space with polyhedral cages having 12 pentagonal faces and k hexagonal faces, denoted $5^{12}6^k$, where k = 0, 2, 3, or 4.[1] The predominant hydrate crystals, sI and sII, comprise small dodecahedral cages (k = 0) and large cages (k = 2 for sI and k = 4 for sII);[1] k = 3 cages are commonly found at hydrate interfaces.[21,40] The size of clathrate nuclei was monitored using the number n of connected clathrate cages, which were identified with the method of ref 38 and clustered according to a distance criterion (0.86 nm guest−guest distance). A typical rare-events strategy to compute the nucleation rate would involve umbrella sampling to obtain the free energy as a function of n.[41] However, we found that both hybrid Monte Carlo/molecular dynamics (MC/MD)[42,43] and equilibrium path sampling (EPS,[27] also known as BOLAS[44]) proved difficult because of the exceptionally slow dynamics of growth and dissolution of the clathrate nuclei. These slow dynamics are due to coupling between nucleus growth/dissolution and transport processes outside the nucleus, including transfer of methane across the solution−gas interface, diffusion of methane through solution, attachment/detachment of methane to the nucleus, and formation/decomposition of water cages. This makes equilibration, decorrelation, and convergence of statistics intractable even with umbrella sampling. To circumvent this issue, we assumed that the free energy as a function of nucleus size n, $F(n)$, has the form suggested by classical nucleation theory (CNT):[41]

$$F(n) = n^{2/3}\phi\gamma - n\Delta\mu \tag{1}$$

where ϕ is a nucleus shape factor (nuclei are assumed to be spherical in CNT), γ is the surface free energy, and $\Delta\mu = k_B T \ln S$ is the chemical potential difference between the metastable (solution) and stable (hydrate) phases. According to CNT, competition between the $n^{2/3}$ (surface) and n (volume) terms gives rise to a maximum in $F(n)$ at the critical nucleus size $n^{\neq}$, where nuclei are equally likely to grow or dissolve; from eq 1, $n^{\neq}$ is given by

$$n^{\neq} = \left(\frac{2\phi\gamma}{3\Delta\mu}\right)^3 \tag{2}$$

We also assumed a CNT expression for the nucleation rate, J:[41]

$$J = \rho Z D \exp[-F(n^{\neq})/k_B T] \tag{3}$$

where ρ is the concentration of monomers in solution; Z is the Zeldovich factor, which depends on $\partial^2 F/\partial n^2$ at $n^{\neq}$; and D is a generalized diffusivity along the nucleus size coordinate,[41] often interpreted as an attachment/detachment frequency. Computational studies have often found that eqs 1−3 are approximately correct[41] when nuclei are large and when microscopic (rather than bulk) values are used for γ and $\Delta\mu$. The definition of a "monomer" depends on the mechanism of growth for the nucleus. If the key step in this process is the adsorption of a single guest molecule on the nucleus, then the monomer population may be taken as the concentration of methane in solution. However, other choices for the monomers are possible, including individual enclathrated methanes in solution. The latter is a self-consistent choice for our framework, as CNT requires that the monomer in solution be the same as the unit used for counting the nucleus size n. The most accurate definition of the monomer is likely somewhere between these two conventions. We defined the monomers as isolated (and occupied) hydrate cages, but our conclusions would not change if other conventions were adopted.

At 273 K and 900 atm, spontaneous formation of isolated hydrate cages is extremely rare. Umbrella sampling along a rings coordinate (five- and six-membered rings of water molecules around a methane molecule) revealed that the reversible work to create a single cage in 729 nm^3 of metastable aqueous methane solution is nearly $20k_BT$. This agrees with previous studies showing that isolated hydrate cages live for only a few picoseconds[45] and that their spontaneous formation is extremely rare.[46]

Seeds of methane hydrate with the stable sI crystal structure were prepared and immersed in solution, where they were equilibrated for 20 ns with a constraint on the nucleus size. These constrained nuclei were the seeds for subsequent unconstrained trajectories at 273 K and 900 atm from which we estimated a critical nucleus size of slightly above 300 cages. An ensemble of equilibrated seed nuclei of size n = 300 was prepared, and then a swarm of short unconstrained trajectories was initiated from each seed. The trajectories resembled a random walk along the nucleus size coordinate that provided an estimate of the diffusivity D from Einstein's relation $\langle(\delta n)^2\rangle = 2Dt$, where $\delta n = n(t) - \langle n(t)\rangle$. The time-dependent drifting mean $\langle n(t)\rangle$ for each swarm was removed to eliminate the bias arising from an imprecise location of the barrier top. The mean squared displacement as a function of time is shown in Figure 2. The transient behavior of $\langle(\delta n)^2\rangle$ as it becomes linear in time is qualitatively similar to results from previous nucleation studies on other systems.[47,48]

dx.doi.org/10.1021/ja309117d | J. Am. Chem. Soc. 2012, 134, 19544−19547

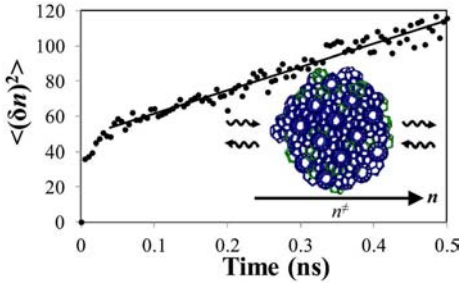

Figure 2. Mean squared displacement $\langle(\delta n)^2\rangle$ along the nucleus size coordinate as a function of time (where $\delta n = n(t) - \langle n(t)\rangle$). The line extends through the portion of data that was used to calculate D, a measure of the attachment/detachment rate of cages to the critical nucleus. D is calculated to be 65 cages^2/ns. The inset shows a representative critical nucleus, with $5^{12}6^2$, $5^{12}6^0$, and $5^{12}6^3$ hydrate cages colored blue, green, and red, respectively. For clarity, methane molecules are not shown.

The drift velocity of n can reveal the last unknown parameter in the expression for the nucleation free energy $F(n)$, namely, the surface free energy γ. With the assumption of overdamped Langevin dynamics along n,[49,50] the drift velocity of n should be proportional to the generalized size-dependent force of Volmer and Weber,[51] $\partial F(n)/\partial n$:

$$\frac{d\langle n\rangle}{dt} = -\frac{D}{k_B T}\frac{\partial F(n)}{\partial n} \quad (4)$$

Mean drift velocities at each size were obtained from unconstrained simulations of equilibrated seeds of various sizes. Figure 3 shows that the chosen seed-nucleus sizes

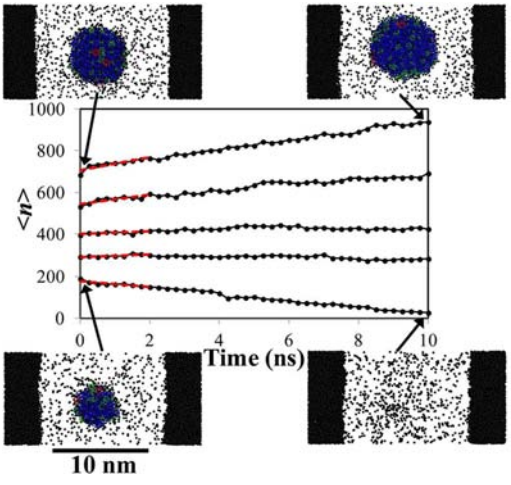

Figure 3. Time evolution of nuclei from unconstrained MD simulations. The red dashed lines indicate the linear fits from which the drift velocities were extracted. The color scheme of simulation snapshots is the same as in Figure 2, except that methane molecules are now shown as black spheres; water molecules of the liquid are not shown.

bracketed $n^{\neq}$: the larger nuclei grew, and the smaller nuclei shrank. The drift velocity for each nucleus size was extracted from a linear fit to the first 2 ns of growth/dissolution (shown as red dashed lines in Figure 3).

Values of $\Delta\mu$, ρ, and D were directly calculated from the simulations. The surface energy γ was estimated as a fitting parameter by least-squares minimization using the drift velocity data in Figure 3. From the values of $\Delta\mu$, ρ, D, and γ, we estimated

Table 1. Quantities in the Nucleation Barrier and Rate Expressions at T = 273 K and P = 900 atm

supersaturation, S	5.8
chemical potential difference, $\Delta\mu/k_BT$	1.76
shape factor, ϕ (m^2)	2.3×10^{-18}
surface energy, γ (mJ/m^2)	31
monomer number density, ρ (cm^{-3})	2.1×10^{10}
Zeldovich factor, Z	0.04
diffusivity, D (cages^2/ns)	65
critical nucleus size, $n^{\neq}$	341
nucleation barrier, $F(n^{\neq})/k_BT$	300
nucleation rate, J (nuclei cm^{-3} s^{-1})	3×10^{-111}

$F(n^{\neq})$, $n^{\neq}$, and J using eqs 1−3, respectively. The obtained values are listed in Table 1.

The unconstrained simulations validated the CNT assumptions that the nuclei are spherical and possess the structure of the sI crystal phase. These findings are consistent with the results of a previous study predicting that hydrate nuclei are always crystalline above ∼270 K.[15]

The solution−hydrate surface energy we obtained, 31 mJ/m^2, agrees extremely well with the experimentally measured value[52] of 32 ± 3 mJ/m^2. A similar estimate of γ can be obtained from the CNT expression for the critical nucleus size $n^{\neq}$ (eq 2). From our seeded trajectories, $n^{\neq}$ is between 300 and 400 cages, which gives γ in the range 29−32 mJ/m^2. A larger but comparable value of 36 ± 2 mJ/m^2 was previously obtained in simulations by fitting to the Gibbs−Thomson equation.[15]

The experimental surface energy[52] is for bulk hydrate at length scales much larger than typical critical nuclei,[53] but the critical nuclei that we observed were exceptionally large, thus displaying bulk-like behavior. The critical nucleus size obtained using γ from the drift velocity regression is 341 cages, which is consistent both internally (given the growth and dissolution behavior observed in Figure 3) and with previous simulations under similar conditions.[15] The critical nuclei in our study had diameters of 5−6 nm and contained 5000−6000 molecules. Studies at higher driving forces found much smaller critical nuclei,[13,14,17] a trend that is in agreement with the predictions of CNT.

The most important prediction from this work is the nucleation rate, which provides a direct comparison with experiment. All previous spontaneous hydrate nucleation simulations were performed with elevated driving forces that gave nucleation rates many orders of magnitude higher than experimental nucleation rates. A previous theoretical treatment of CO_2 hydrates derived a hydrate−solution surface energy of ∼10 mJ/m^2 to match the experimental crystallization rate assuming that nucleation occurs homogeneously.[54] We come to a different conclusion: the surface energy is in fact large, almost identical to the value of 32 mJ/m^2 for the ice−liquid interface,[52] resulting in extremely large nucleation barriers of ∼300k_BT at the moderate temperatures and pressures for which methane clathrates form in pipelines, nature, and the laboratory. Our simulations predict that the homogeneous nucleation rate is vanishingly small, on the order of 10^{-111} nuclei cm^{-3} s^{-1}. At this rate, even with all the water in the world's oceans, the induction time to see one nucleus form homogeneously would be 10^{80} years! This strongly suggests that the induction times reported in experiments cannot originate from homogeneous nucleation events.

Gas hydrates form on seafloor sediment, permafrost, pipelines, and high-pressure lab equipment. Future experiments that can

clearly discriminate between homogeneous and heterogeneous nucleation would be extremely useful for understanding nucleation in these realistic environments. Likewise, future simulations should probe hydrate nucleation by heterogeneous nucleation mechanisms, such as the effect of mineral surfaces.[55] Plausible mechanisms by which surfaces could increase the nucleation rate involve preferential binding of partial or complete clathrate cages at surfaces, enhanced guest concentration at the surface (as seen in both experiments[56] and simulations[55] and perhaps best understood as a preferential binding effect[57]), stabilization of water-separated methane pairs, or a favorable surface–hydrate free energy. Studies to identify specific surfaces that catalyze nucleation and perhaps coatings that can inhibit hydrate nucleation would also be interesting directions for future research.

■ ASSOCIATED CONTENT

Supporting Information

Methods, force-field parameters, and calculation details. This material is available free of charge via the Internet at http://pubs.acs.org.

■ AUTHOR INFORMATION

Corresponding Author

baronp@engineering.ucsb.edu

Notes

The authors declare no competing financial interest.

■ ACKNOWLEDGMENTS

We gratefully acknowledge support from the National Science Foundation through CHE-1125235 (B.P. and V.M.) and CBET-1159746 (M.F.D.). We thank the Center for High Performance Computing at the University of Utah for allocation of computing time.

■ REFERENCES

(1) Sloan, E. D., Jr. *Nature* **2003**, *426*, 353.
(2) Koh, C. A.; Sloan, E. D.; Sum, A. K.; Wu, D. T. *Annu. Rev. Chem. Biomol. Eng.* **2011**, *2*, 237.
(3) Hesselbo, S. P.; Grocke, D. R.; Jenkyns, H. C.; Bjerrum, C. J.; Farrimond, P.; Bell, H. S. M.; Green, O. R. *Nature* **2000**, *406*, 392.
(4) Brewer, P. G.; Friederich, C.; Peltzer, E. T.; Orr, F. M. *Science* **1999**, *284*, 943.
(5) Florusse, L. J.; Peters, C. J.; Schoonman, J.; Hester, K. C.; Koh, C. A.; Dec, S. F.; Marsh, K. N.; Sloan, E. D. *Science* **2004**, *306*, 469.
(6) Lee, H.; Lee, J. W.; Kim, D. Y.; Park, J.; Seo, Y. T.; Zeng, H.; Moudrakovski, I. L.; Ratcliffe, C. I.; Ripmeester, J. A. *Nature* **2005**, *434*, 743.
(7) Anderson, B. J.; Bazant, M. Z.; Tester, J. W.; Trout, B. L. *J. Phys. Chem. B* **2005**, *109*, 8153.
(8) Jensen, L.; Thomsen, K.; von Solms, N.; Wierzchowski, S.; Walsh, M. R.; Koh, C. A.; Sloan, E. D.; Wu, D. T.; Sum, A. K. *J. Phys. Chem. B* **2010**, *114*, 5775.
(9) Conde, M. M.; Vega, C. *J. Chem. Phys.* **2010**, *133*, No. 064507.
(10) Handa, Y. P.; Tse, J. S.; Klug, D. D.; Whalley, E. *J. Chem. Phys.* **1991**, *94*, 623.
(11) Hawtin, R. W.; Quigley, D.; Rodger, P. M. *Phys. Chem. Chem. Phys.* **2008**, *10*, 4853.
(12) Vatamanu, J.; Kusalik, P. G. *Phys. Chem. Chem. Phys.* **2010**, *12*, 15065.
(13) Walsh, M. R.; Koh, C. A.; Sloan, E. D.; Sum, A. K.; Wu, D. T. *Science* **2009**, *326*, 1095.
(14) Jacobson, L. C.; Hujo, W.; Molinero, V. *J. Am. Chem. Soc.* **2010**, *132*, 11806.
(15) Jacobson, L. C.; Molinero, V. *J. Am. Chem. Soc.* **2011**, *133*, 6458.
(16) Debenedetti, P. G.; Sarupria, S. *Science* **2009**, *326*, 1070.
(17) Radhakrishnan, R.; Trout, B. L. *J. Chem. Phys.* **2002**, *117*, 1786.
(18) Moon, C.; Taylor, P. C.; Rodger, P. M. *J. Am. Chem. Soc.* **2003**, *125*, 4706.
(19) Guo, G. J.; Li, M.; Zhang, Y. G.; Wu, C. H. *Phys. Chem. Chem. Phys.* **2009**, *11*, 10427.
(20) Christiansen, R. L.; Sloan, E. D., Jr. *Ann. N.Y. Acad. Sci.* **1994**, *715*, 283–305.
(21) Vatamanu, J.; Kusalik, P. G. *J. Am. Chem. Soc.* **2006**, *128*, 15588.
(22) Liang, S.; Kusalik, P. G. *J. Phys. Chem. B* **2010**, *114*, 9563.
(23) Sarupria, S.; Debenedetti, P. G. *J. Phys. Chem. A* **2011**, *115*, 6102.
(24) English, N. J.; Johnson, J. K.; Taylor, C. E. *J. Chem. Phys.* **2005**, *123*, No. 244503.
(25) Rodger, P. M. *Gas Hydrates: Challenges for the Future* **2000**, *912*, 474.
(26) Chihaia, V.; Adams, S.; Kuhs, W. F. *Chem. Phys.* **2005**, *317*, 208.
(27) Peters, B.; Zimmermann, N. E. R.; Beckham, G. T.; Tester, J. W.; Trout, B. L. *J. Am. Chem. Soc.* **2008**, *130*, 17342.
(28) English, N. J.; Tse, J. S. *Phys. Rev. Lett.* **2009**, *103*, No. 015901.
(29) Walsh, M. R.; Beckham, G. T.; Koh, C. A.; Sloan, E. D.; Wu, D. T.; Sum, A. K. *J. Phys. Chem. C* **2011**, *115*, 21241.
(30) Abay, H. K.; Svartaas, T. M. *Energy Fuels* **2011**, *25*, 42.
(31) Herri, J. M.; Pic, J. S.; Gruy, F.; Cournil, M. *AIChE J.* **1999**, *45*, 590.
(32) Lekvam, K.; Ruoff, P. *J. Am. Chem. Soc.* **1993**, *115*, 8565.
(33) Devarakonda, S.; Groysman, A.; Myerson, A. S. *J. Cryst. Growth* **1999**, *204*, 525.
(34) Takeya, S.; Hori, A.; Hondoh, T.; Uchida, T. *J. Phys. Chem. B* **2000**, *104*, 4164.
(35) Jensen, L.; Thomsen, K.; von Solms, N. *Chem. Eng. Sci.* **2008**, *63*, 3069.
(36) Molinero, V.; Moore, E. B. *J. Phys. Chem. B* **2009**, *113*, 4008.
(37) Jacobson, L. C.; Molinero, V. *J. Phys. Chem. B* **2010**, *114*, 7302.
(38) Jacobson, L. C.; Hujo, W.; Molinero, V. *J. Phys. Chem. B* **2009**, *113*, 10298.
(39) Dyadin, Y. A.; Aladko, E. Y.; Larionov, E. G. *Mendeleev Commun.* **1997**, *7*, 34.
(40) Nguyen, A. H.; Jacobson, L. C.; Molinero, V. *J. Phys. Chem. C* **2012**, *116*, 19828.
(41) Auer, S.; Frenkel, D. *Annu. Rev. Phys. Chem.* **2004**, *55*, 333.
(42) Duane, S.; Kennedy, A. D.; Pendleton, B. J.; Roweth, D. *Phys. Lett. B* **1987**, *195*, 216.
(43) Forrest, B. M.; Suter, U. W. *J. Chem. Phys.* **1994**, *101*, 2616.
(44) Radhakrishnan, R.; Schlick, T. *J. Chem. Phys.* **2004**, *121*, 2436.
(45) Guo, G. J.; Zhang, Y. G.; Zhao, Y. J.; Refson, K.; Shan, G. H. *J. Chem. Phys.* **2004**, *121*, 1542.
(46) Guo, G. J.; Zhang, Y. G.; Li, M.; Wu, C. H. *J. Chem. Phys.* **2008**, *128*, No. 194504.
(47) Auer, S.; Frenkel, D. *J. Chem. Phys.* **2004**, *120*, 3015.
(48) Lundrigan, S. E. M.; Saika-Voivod, I. *J. Chem. Phys.* **2009**, *131*, No. 104503.
(49) Zwanzig, R. *Nonequilibrium Statistical Mechanics*; Oxford University Press: New York, 2001.
(50) Wedekind, J.; Reguera, D. *J. Phys. Chem. B* **2008**, *112*, 11060.
(51) Volmer, M.; Weber, A. *Z. Phys. Chem.* **1926**, *119*, 277.
(52) Anderson, R.; Llamedo, M.; Tohidi, B.; Burgass, R. W. *J. Phys. Chem. B* **2003**, *107*, 3507.
(53) Lovette, M. A.; Browning, A. R.; Griffin, D. W.; Sizemore, J. P.; Snyder, R. C.; Doherty, M. F. *Ind. Eng. Chem. Res.* **2008**, *47*, 9812.
(54) Zhang, J. F.; Di Lorenzo, M.; Pan, Z. J. *J. Phys. Chem. B* **2012**, *116*, 7296.
(55) Liang, S.; Rozmanov, D.; Kusalik, P. G. *Phys. Chem. Chem. Phys.* **2011**, *13*, 19856.
(56) Boewer, L.; Nase, J.; Paulus, M.; Lehmkuhler, F.; Tiemeyer, S.; Holz, S.; Pontoni, D.; Tolan, M. *J. Phys. Chem. C* **2012**, *116*, 8548.
(57) Kirkwood, J. G.; Goldberg, R. J. *J. Chem. Phys.* **1950**, *18*, 54.